Renewable Energy 199. (2022): 895-907

DOI: https://doi.org/10.1016/j.renene.2022.09.021

AQUEOUS-PHASE REFORMING OF WATER-SOLUBLE COMPOUNDS FROM PYROLYSIS BIO-OILS

Jéssica Justicia, José Alberto Baeza, Adriana S. de Oliveira, Luisa Calvo, Francisco Heras*, Miguel A. Gilarranz

Chemical Engineering Department. Universidad Autónoma de Madrid. Ciudad Universitaria de Cantoblanco. 28049 Madrid (Spain)

*Corresponding author: fran.heras@uam.es

Abstract

Aqueous-phase reforming (APR) of model compounds of bio-oil aqueous fraction (AFB) was studied at different operating conditions. Substrate conversion, carbon-to-gas yield (CCgas) and hydrogen and alkanes production were evaluated. Levoglucosan, hydroxyacetone, furfural and acetic acid were selected as representative of AFB and tested in batch APR at different concentrations (1-5 %wt.), temperatures (175-220 ^{o}C) and reaction times (0.5-4 h), using 3% (wt.) Pt/CB catalysts. Best results were obtained at 220 ^{o}C and 1 %, with 70-90 % substrate conversions, 45-70 % CC gas and hydrogen production up to 50 mmol per gram of total organic carbon (TOC). Catalyst stability was checked in APR of levoglucosan during five successive 4 h reaction cycles. The catalyst exhibited high stability, CCgas remained constant and hydrogen production increased and became stable after first reaction cycle with only a slight decrease of TOC conversion. The catalyst with well dispersed metal phase and high contribution of nanoparticles smaller than 2 nm showed a higher production of hydrogen. APR was proved to be a feasible option for the valorisation of AFB.

Keywords

Aqueous-phase reforming, bio-oil, aqueous fraction, water soluble, hydrogen, Pt/C catalyst

1. Introduction

With the focus in a decarbonized future, research in waste biomass valorisation has received increasing attention [1]. One of the most promising valorisation methods is pyrolysis [2], which produces three product streams: gas (mainly composed by CO, CO_2, CH_4 and H_2), bio-oil and biochar. Several works have been focused on the production of gas, due to its good properties for use as biofuel, and biochar, which can be used as fuel, adsorbent, soil amendment, etc. [3-5]. The recovery and use of bio-oil is more challenging because it is composed of an organic and an aqueous fraction, both containing a complex mixture of compounds [6].

The organic fraction of bio-oil contains mainly phenolic compounds and lignin derivatives, including hydroxymetilfurane, phenol and phenolic compounds (guaiacol, cresol, etc.), organic acids (hexadecenoic, octadecanoic) and methyl esters of these acids, among others [1,7,8]. The composition of bio-oil aqueous fraction (AFB) is highly variable, depending mainly on the starting biomass and the pyrolysis conditions. However, most works in literature reported a reduced number of components as the most frequent, namely levoglucosan, acetic acid, furfural and hydroxyacetone (acetol). Table 1 shows proximate quantitative composition of AFBs obtained from different types of biomass. The water content in all cases is as high as 80-90 %, and none

of the four main components appears in a concentration higher than 5 % (wt.), although their concentration can change substantially depending on the initial biomass used. Remon et al. [9] studied the aqueous phase of the bio-oil produced by fast pyrolysis of pine wood in fluidized bed and spouted bed reactors, observing similar composition in both cases, with levoglucosan and hydroxyacetone as the components at higher concentration. In the case of the work by Black et al. [10] on fast pyrolysis of oak wood the main components of AFBs were levoglucosan and acetic acid.

Table 1: *Characterization of aqueous fraction of bio-oil obtained for different biomass*

	Composition (%, wt.)				
BIOMASS	OAK WOOD		PINE SAWDUST		
Hydroxyacetone	0.3	0.1	1.4	0.7	1.5
Levoglucosan	1.1	4.5	3.1	2.0	1.6
Acetic acid	0.6	3.1	3.1	0.7	0.7
Furfural	< 0.2	0.2	< 0.9	0.1	<0.1
Water	89.9	80.6	82.0	84.0	84.0
Ref.	[11]	[10]	[12]	[9]	[9]

The composition and high water content of AFB poses important challenges for the valorisation and recovery of the chemicals contained in this fraction. Thus, the use of AFB as biofuel would require costly removal of water. In this context, aqueous-phase reforming (APR) can be considered a promising method for the valorisation of AFB. As in the case of steam reforming (SR), APR consists essentially in the reaction between an organic substrate and water to produce hydrogen and carbon monoxide, but in APR the reaction takes place in the liquid phase [13]. In terms of energy, APR of AFB can be more efficient than steam reforming (SR) because milder operating conditions are used (200-250 °C and 15-30 bar) and evaporation of the feed is not needed [14,15]. At APR conditions the water gas shift reaction (WGS) equilibrium is almost completely displaced to products, yielding a gas product mainly composed by hydrogen and carbon dioxide [16-18]. In addition to reforming and WGS reactions, additional reactions occurring at APR conditions leading to the production of different water-soluble hydrocarbons via Fischer-Tropsch route, hydrogenation and dehydration [19,20]. APR process can be considered to involve two main routes, namely i) C-C, C-H and O-H bonds cleavage and WGS; and ii) C-O bonds rupture and alkane and formation of carbohydrates such as acids, sugar alcohols, etc. [19,21,22].

Regarding catalysts for APR, the most studied have been Group VIII to X metals due to higher activity in C-C bond cleavage [23-25]. The best results in terms of catalytic activity and selectivity to hydrogen have been found using supported Ni and Pt, with Pt showing much higher stability [18,21,26]. The support also plays an essential role in APR process. In general, acidic and neutral supports promote secondary reactions leading to alkane formation, while basic supports favor WGS and other reactions that increase hydrogen yield [27]. γ-Al_2O_3 has been one of the most widely studied supports for Pt catalysts showing high hydrogen selectivity, although hydration of this material to boehmite at APR conditions leads to an increase in selectivity to alkanes and eventually results in loss of activity [28,29 30]. Carbon materials have also been shown as interesting supports for APR catalysts because of their tunable textural and chemical structure and thermal stability [30-32].

The most studied APR substrates have been sugar alcohols, including sorbitol, xylitol and glucose, and alcohols, such as glycerol, methanol and ethanol, among others [16,17,33,34]. A higher suitability for hydrogen production has been attributed to substrates with a C:O atomic ratio close to 1 [20].

In the last years, the APR of bio-derived compounds, especially from biorefinery schemes, has received increasing attention. Some works have studied the APR of individual compounds commonly present in bio-oil and AFB. Hydroxyacetone has been one of the most studied model compounds. Some works showed carbon yield to gases of up to 50 % in the APR of hydroxyacetone using Ni-Co/Al-Mg catalysts and H_2 content in produced gas higher than 30 % [35]. However, hydroxyacetone can also undergo aldol condensation reactions leading eventually to catalyst deactivation by coke formation in Pt/AlO(OH) and Pt/ZrO_2 catalysts [36]. Substantially different results were reported in other works where only 1-2 % carbon to gas yield was observed using Ni catalysts supported on alumina, ceria and lanthana [37]. Diverse results have also been reported for the APR of acetic acid, which is among the most refractory compounds in AFB. Nozawa et al. [38] compared the APR of ethanol and acetic acid using Ru/TiO_2 catalysts, achieving four times higher values of TOF for hydrogen production in the case of ethanol. Similar trends were shown by Arandia et al. [39] for the APR of acetic acid and ethanol catalysed by spinel $NiAl_2O_4$, Ni/CeO_2-γAl_2O_3 and Ni/La_2O_3-αAl_2O_3. Some studied have reported that catalyst deactivation in the APR of acetic acid and ethanol is not relevant [39]. However, Lozano et al. [35], found low reactivity of acetic acid in APR using Ni-Co/Al-Mg catalysts, especially compared to ethanol, due to catalyst deactivation.

As reported in literature, one the main obstacles for the use of APR a hydrogen source is the cost of the organic compounds used as process feedstock. On the other hand, the high water-content and wide composition in organic matter of AFB makes difficult to develop routes for its valorization or recovery of components, therefore it is usually considered as a wastewater stream. The current work proposes overcoming both obstacles through the valorization of AFB by APR to produce biomass-derived hydrogen and alkanes. Processability of different components of AFB is study to determine most favorable compositions for APR process. Likewise, catalyst stability is evaluated since deactivation is a common bottleneck in the valorization of complex biomasses by APR.

Despite the works commented above, few studies can be found in literature comparing the behavior in APR of main compounds occurring in biorefinery waste streams feeds. The objective of the current work is to explore the APR of bio-oil aqueous fraction with carbon-supported Pt catalysts expanding the number of model compounds considered to assess the role in the processability of AFB. The stability of the catalysts was also evaluated upon five successive applications.

2. Experimental section

2.1 Materials

The chemicals used as bio-oil aqueous fraction model compounds were furfural (98 %), levoglucosan (98 %), hydroxyacetone (95 %) and acetic acid (99 %) supplied by Merck, Carbosynth Limited, Alfa-Aesar-Thermofisher and Sigma Aldrich, respectively. Hexachloroplatinic acid solution (8 % wt. in water) purchased from Sigma Aldrich was used as

precursor salt for catalysts preparation, while carbon black ENSACO 250G supplied by Timcal Canada Inc. (Canada) was used as catalyst support.

On the other hand, ENSACO 250G support is characterized by a relatively ordered structure, which contributes to hydrothermal stability. Likewise, the absence of oxygen in the APR medium minimizes carbon support degradation [40].

2.2 Synthesis and characterization of catalyst

3 % (wt.) Pt/CB catalyst was prepared by incipient wetness impregnation. The support was impregnated with the chloroplatinic acid aqueous solution, dried overnight at 60 °C, calcined in air at 200 °C for two hours and, finally, reduced under H_2 flow at 300 °C for two hours. This catalyst was selected due to the high activity shown in previous works on the APR of biomass pollutants in wastewater [41]. A 3% (wt) nominal metal load was considered as suitable for assessing the suitability of AFB as a substrate for APR according to the results achieved in previous works on the APR of a variety of substrates [41,60,64].

Fresh catalyst was characterized by N_2 adsorption/desorption at 77 K (Tristar II, Micromeritics). TPD/TPO analyses were performed with TA Instruments SDT 650. TPD were carried out under 50 mL/min N_2 flow, from room temperature to 900 °C using a ramp of 10 °C/min; next, the samples were cooled up to 100 °C and by last, the gas was switched to air without flowrate variation to accomplish the TPO up to the same final temperature using a 5 °C/min ramp. Fresh and used catalysts reduced for 2h were characterized by STEM with a Tecnai F30 microscope (FEI company). Those that were reduced for 3h, with a FEI Talos F200X microscope. Software 'ImageJ 1.51k' was used for counting and measuring Pt nanoparticles on digital STEM images. XPS profiles were recorded using a PHI VersaProbe II instrument equipped with X-ray source, 1486.6 eV at 25.1 W, with a beam diameter of 100.0 µm. Software 'XPS peak v4.1' was used for the deconvolution of the spectra to obtain the relative amounts of Pt^{n+} and Pt° species. The data analysis procedure involved smoothing, a Shirley background subtraction and mixed Gaussian–Lorentzian by a least-square method for curve fitting. C 1s peak (284.6 eV) was used as internal standard for binding energies corrections due to sample charging.

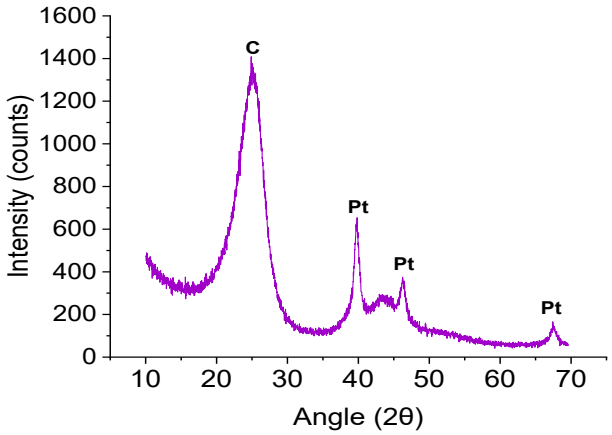

Figure 1: *XRD spectrum of Pt/CB catalyst*

XRD pattern (Figure 1) was obtained by a Bruker D8 Discover device using monochromic CuKα radiation, an angular range of 20 to 70°, a step size of 0.02° and a dwell time of 1 s per increment. The broad peak at 25.0° corresponds to (002) band of carbon black support, showing that is

predominantly an amorphous carbon, although the peak around 44° is usually ascribed to (200) band and is indicative of small regions with graphitic properties [42]. The sharp peaks at 39.9, 46.5° and 67.6° can be attributed to platinum reflections (111), (200) and (220), respectively, which are consistent with a face centred cubic structure, showing the formation of crystalline Pt phase [13,43].

The N_2 adsorption/desorption isotherm and pore size distribution determined from the isotherm by BJH method are shown for the catalyst in Figures 2 and 3, respectively. The isotherm obtained corresponds to type IV-a according to IUPAC classification, showing very low contribution of microporosity. The BET specific surface area (S_{BET}), external area (A_{ext}) and pore volume of the fresh catalyst and the support are summarized in Table 2. The textural properties of the catalyst are the same to those of the carbon black support, i.e., low specific surface area and microporosity, but noticeable mesoporosity (0.09 cm^3/g). A relatively wide pore size distribution was obtained in the narrow mesopore range, extending well beyond 12 nm, with a substantial contribution between 2 and 4 nm. The small particle size (22 µm) and negligible microporosity of the catalysts and the use of a slurry reactor provided with mechanical stirring contribute to diminished mass transfer constraints.

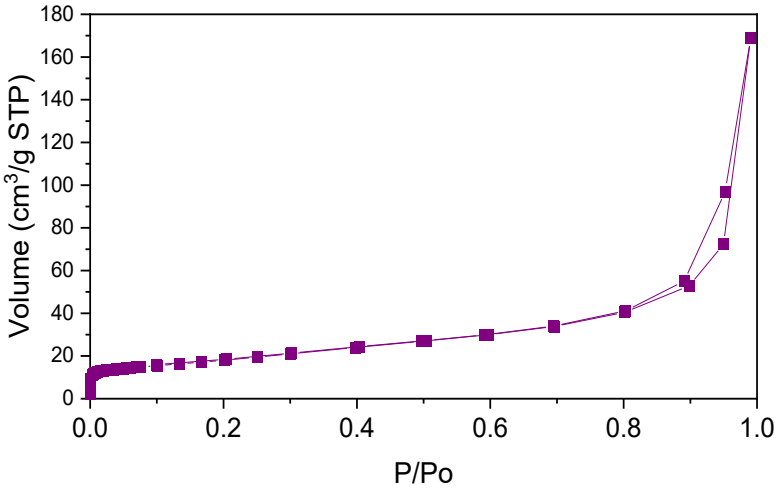

Figure 2: *N_2 adsorption/desorption isotherm at 77 K for fresh catalyst.*

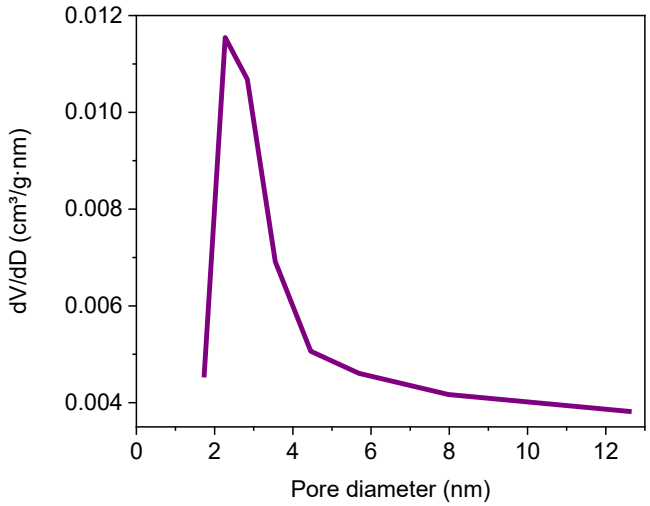

Figure 3: *Pore size distribution (BJH Desorption) for fresh catalyst.*

Table 2: *Characterization of support and catalyst used in APR experiments*

Catalyst	S_{BET} (m^2/g)	A_{ext} (m^2/g)	Micropore volume (cm^3/g)	Mesopore volume (cm^3/g)	pH slurry
Pt/CB	65	65	< 0.001	0.09	8.7
CB	65	65	< 0.001	0.09	8.9

2.3. APR experiments

The reaction experiments were carried out in a 50 mL Teflon-lined stainless steel reactor vessel that was inserted in a heating block. The reactor was loaded with 15 mL of initial solution and 0.15 g of catalyst. Then, it was sealed and purged three times with Ar. Initial pressure at room temperature was set at 5 bar and magnetic stirring at 750 rpm. The reactor was heated to reaction temperature using a 3 °C/min ramp. After completion of the reaction time, the reactor was cooled down to room temperature. The gas produced was collected in multilayer foil sample bags (Supelco, USA) and analysed in a GC/FID/TCD apparatus (7820 A, Agilent) using two packed columns and a molecular sieve column. The liquid phase produced was characterized by measuring total organic carbon (TOC) with a TOC-VCSH apparatus (Shimadzu).

Previous works on the APR of other substrates using the same catalyst Pt/C indicated good reproducibility of the results. Thus, in APR of brewery and juice production wastewaters, error values were around 5-10 % and 10-20% for X_{TOC} and gas product composition, respectively [60,64].

TOC conversion (X_{TOC}), carbon conversion to gas (CC gas), H_2 yield (Y_{H2}), H_2 selectivity (S_{H2}) and alkanes selectivity ($S_{ALKANES}$) were calculated as:

$$X_{TOC}\ (\%) = \frac{TOC_{initial}\ (\frac{mg}{L}) - TOC_{final}\ (\frac{mg}{L})}{TOC_{initial}\ (\frac{mg}{L})}\ x\ 100 \quad (1)$$

$$CC\ gas\ (\%) = \frac{C_{gas}\ (g)}{C_{initial}\ (g)}\ x\ 100 \quad (2)$$

$$Y_{H2} = \frac{H_2\ produced\ (mol)}{H_2\ theoretical\ (mol)}\ x\ 100 \quad (3)$$

$$S_{H2}\ (\%) = \frac{H_2\ produced\ (mol)}{C_{at\ produced}\ (mol)} x\ \frac{1}{R}\ x\ 100 \quad (4)$$

$$S_{ALKANES} = \frac{Alkanes\ produced\ (mol)}{C_{gas}\ produced\ (mol)}\ x\ 100 \quad (5)$$

3. Results and discussion

3.1 Selection of operating conditions for APR

Temperature, time and feedstock concentration were studied as the main variables affecting the APR process. Furfural was selected as model compound for assessing their influence. TOC conversion, CC gas and gas composition for the treatment of furfural aqueous solutions at different temperature, time and concentration are shown in Figure 4 and Figure 5. Yield and selectivity for 1 % (wt.) furfural APR can be observed in Table 3.

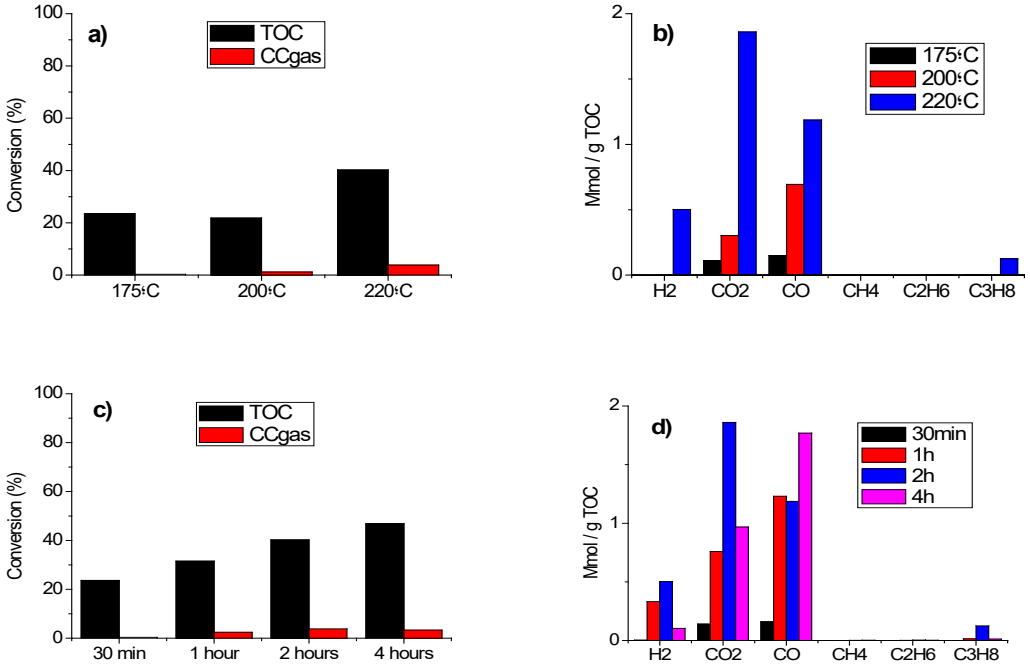

Figure 4: *TOC conversion, CC gas and gas production at: a) and b) different temperature (5 % furfural, 2 h) and c) and d) different time (5 % furfural, 220 °C)*

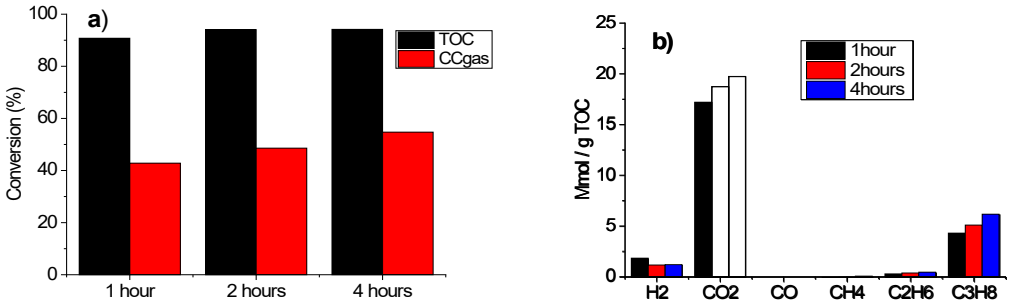

Figure 5: *TOC conversion, CC gas and gas production at different time (1 % furfural, 220 °C)*

In Figures 4a and 4b the results of runs at different temperatures are compared. At 175 and 200 °C, CCgas was almost negligible, even though significant TOC conversion could be observed. TOC conversion could be ascribed to the removal of furfural from the liquid phase by intermolecular aldol condensation and further deposition [44]. Likewise, some removal of furfural by hydrothermal carbonization can be expected from the production of CO and CO_2, particularly at 200 and 220 °C [41,45]. At 220 °C, TOC conversion increased to 49 % and CCgas reached around 5 % (Figure 1a). Figure 4b also show the increase in the production of gases at 220 °C. In all the experiments CO production was higher than the usual values reported for APR, indicating lack of activity of the catalyst in WGS reaction. This could be related to the deposition of condensation products leading to blockage of active sites. An operating temperature of 220 °C was selected for further runs in the view of the gas production achieved.

To assess changes in activity, experiments at different reaction times were carried out. As can be observed in Figures 4c and 4d, TOC removal reached ca. 24 % after 30 min of reaction, however no significant production of hydrogen and alkanes was detected. Significant CO and CO_2 production was recorded at 30 min, probably indicating early occurrence of reactions leading to condensation and hydrothermal carbonization. Steady conversion of TOC with reaction time was observed. Production of gases also increased, but more significantly in the case of CO and CO_2. It must be noted that figures 4 a)-d) show negligible production of methane and ethane, while in former works these gases were produced together with hydrogen in APR of biomass waste compounds [46]. This observation, and the production of CO, suggest constrains for APR reaction, probably due to blockage of active sites at the catalyst. Some authors have previously discussed that polymerization of furfural in an acid medium can result in low hydrogen production [47]. Interestingly, hydrogen is produced despite the lack of activity of the catalyst in WGS reaction. Hydrogen production could be ascribed, at least partially, to a route related to hydrothermal carbon [41].

Condensation reactions leading to blockage of active sites may be promoted by a high concentration of furfural in the reaction medium, therefore additional experiments were carried out with an initial concentration of 1 % (wt.). As can be seen in Figures 5a and 5b, significantly higher TOC conversion and CC gas values of around 95 % and 50 %, respectively, were obtained, with a relatively low influence of reaction time. This boost in conversion at low concentration feedstock has also been observed in the APR of other substrates [41,48]. CO_2 and alkanes production were an order of magnitude higher than when 5 % (wt.) furfural was used. This observation is in agreement with the studies carried out by Luo et al. [48], who studied the APR

of 5 and 10 % (wt.) glycerol with Pt-γAl_2O_3 and observed better results for 5 % solution, in terms of CCgas and hydrogen yield.

The decrease in feed concentration leads negligible presence of CO in gas product stream, showing higher activity of the catalyst in WGS reaction, which also contributes to higher H_2 production. Anyhow, H_2 production and selectivity showed low values for the experiments with 1 % (wt.) furfural, about 1 mmol/gTOC and 2 %, respectively (Figure 5 and Table 3). A fraction of the hydrogen produced may be consumed by the furfural side reactions to produce alkanes, in particular propane as shown by gas analysis. Thus, furfural can be hydrogenated in successive reactions to pentane-1,5-diol, with furfuryl alcohol as reaction intermediate [49]. This C5 diol can undergo in turn dehydrogenation/decarbonylation to produce propane [50]. It must be noted that H_2 production was lower than that of alkanes, which is unusual in APR, particularly for Pt catalysts [18,51,52]. Propane production can be considered as an advantage for a hypothetical energy recovery from the gas by combustion.

Table 3: *Yield and selectivity in the APR of 1 % (wt.) furfural at different times (220 °C)*

Time (h)	Y_{H2} (%)	S_{H2} (%)	$S'_{ALKANES}$ (%)
1	1.0	3.4	19.3
2	0.6	1.6	21.5
4	0.7	1.5	23.8

3.2. APR of individual model compounds

The APR of the main components considered for AFB model composition, i.e. furfural, levoglucosan, acetic acid and hydroxyacetone, was studied using the operating conditions selected from the results of the previous experiments with furfural: 1 % (wt.) concentration and 220 °C.

Figures 6a, 6b and 6c compare TOC conversion and CCgas at different reaction time. A behaviour similar to that of furfural was observed for hydroxyacetone (Figure 6a). TOC conversion for this compound increased with reaction time and reached a maximum value c.a. 79 % after 4 h, which is slightly lower than for furfural, however, a CCgas value as high as 67 % was obtained at this reaction time. The results of levoglucosan APR were strongly dependent on reaction time (Figure 6b). TOC conversion increased from 6.7 at 1 h to 90 % at 4 h. Moreover, CCgas increased from 8 % after 1 h to 10 % after 2 h, whereas an increase to 46 % occurred during the last 2 h of reaction. Finally, relatively high conversion of TOC and CCgas were achieved for acetic acid APR (Figure 6c), reaching in both cases values close to 65 % after 4 h. The CCgas value obtained at 2 h of reaction (49 %) for acetic acid is higher than that reported in other works (33.5 % [53]) using a Pt/C catalyst and a similar feed concentration (0.9 %), probable due to the higher catalyst/feed ratio used in the current work (10 g catalyst/L vs 5 g catalyst/L). Previous works [54] have also shown that catalyst/acetic acid ratio is an important variable influencing APR of this compound.

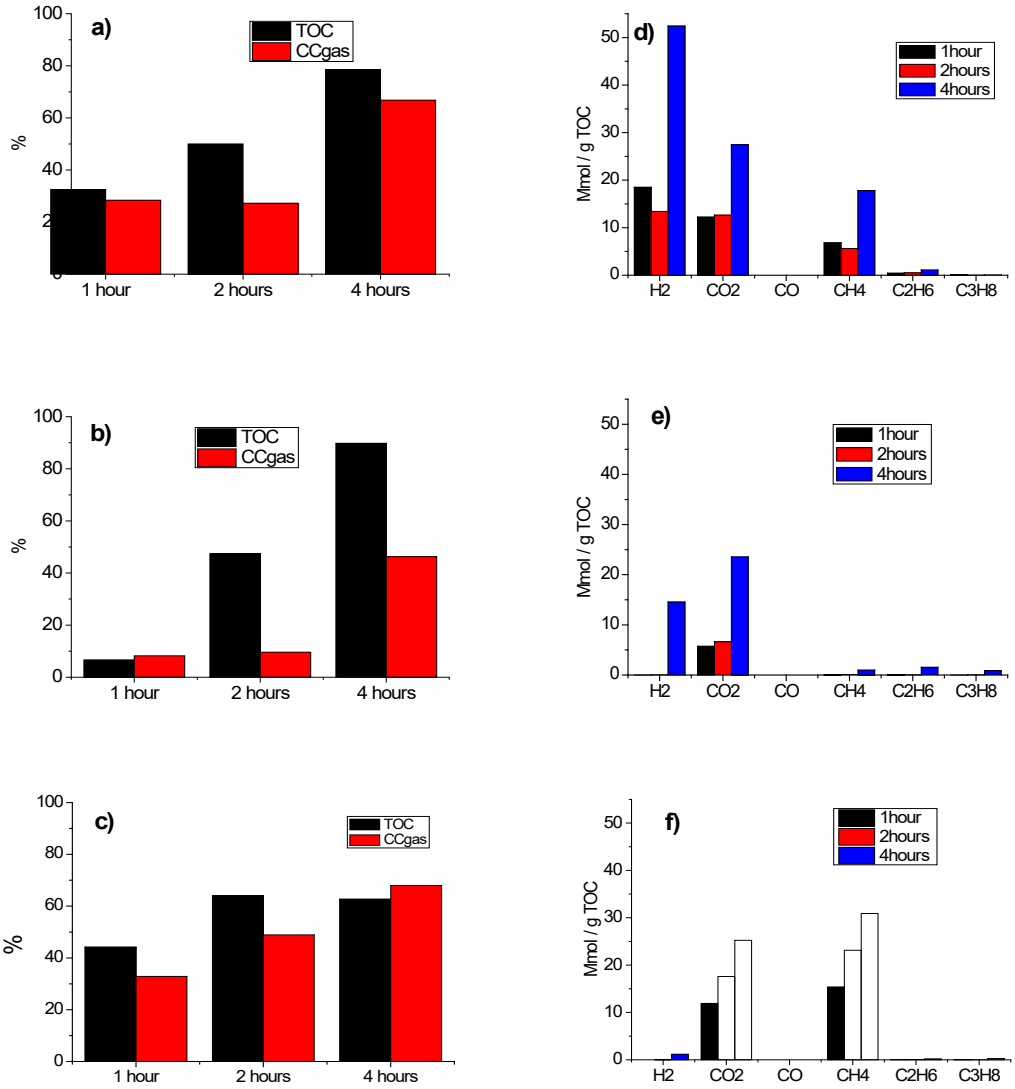

Figure 6: *TOC conversion, CC gas and gas production at different reaction times a) d) Hydroxyacetone, b) e) Levoglucosan, c) f) Acetic acid (1% concentration, 220 °C)*

Table 4: *Yield and selectivity in the APR of model compounds (1% concentration, 220 °C)*

	Time (h)	Y_{H2} (%)	S_{H2} (%)	$S'_{ALKANES}$ (%)
Hydroxyacetone	1	12.3	39.3	19.3
	2	10.2	29.5	19.3
	4	34.9	46.9	18.5
Levoglucosan	1	n.d.	n.d.	n.d.
	2	n.d.	n.d.	n.d.
	4	8.5	24.0	8.5
Acetic acid	1	n.d.	n.d.	56.4
	2	n.d.	n.d.	56.7
	4	0.7	1.0	54.2

Figures 6d, 6e and 6f show individual gases production per gram of TOC at different reaction times and Table 4 the yield and selectivity data. Regarding hydroxyacetone, a sharp increase in hydrogen production can be observed with reaction time, from 15 mmol/gTOC at 2 h to more than 50 mmol/gTOC at 4 h. Alkane fraction was mainly composed by methane, whose production reached 20 mmol/gTOC after 4 h of reaction (Figure 6d). In addition, very high hydrogen selectivity (50 %) was obtained at long reaction time (Table 4). The mechanism of hydroxyacetone APR has been previously discussed as part of the overall reaction mechanism of glycerol APR [55]. This mechanism (Figure 7) would explain the production of hydrogen and methane from hydroxyacetone. Hydroxyacetone can be hydrogenated in several stages to produce methane in the gas phase and undergo hydrogenolysis to generate hydrogen and acetic acid, which in turn can produce more methane [54]. Other authors also reported results of hydroxyacetone reforming, showing the presence of both gases, hydrogen and methane [56-58].

Comparing the results obtained in the current work with those reported in literature, Lozano et al. [35] observed CCgas values of 45-50 % and hydrogen content in the gas of 33.7 % using different catalyst load and similar operating conditions. Callison et al. [55] reported lower hydrogen production values (0.4 mmol H_2 and 0.2 mmol CH_4 vs 5.75 mmol H_2 and 1.96 mmol CH_4), using similar reaction conditions but much higher initial hydroxyacetone concentration (10 vs 1% wt.).

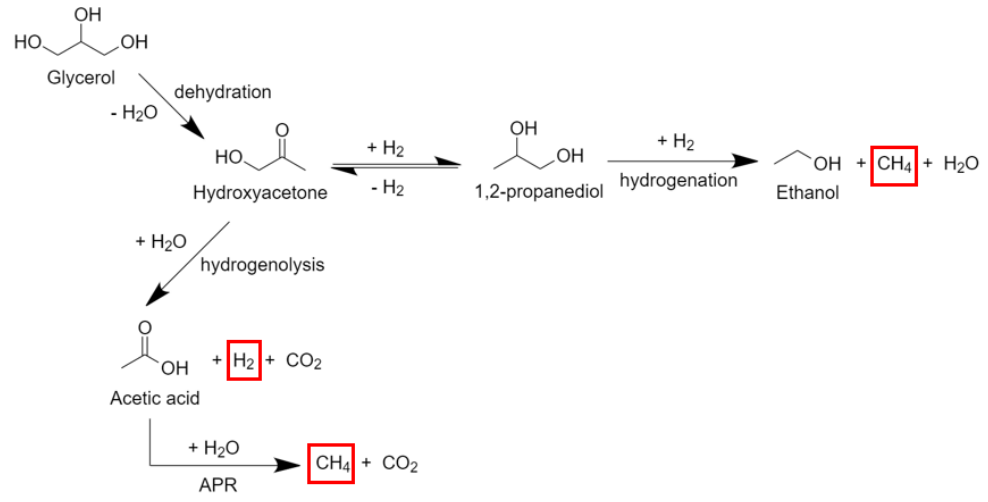

***Figure 7**: Mechanism of glycerol APR [50]*

In the case of levoglucosan, the production of alkanes was negligible after 1 and 3 h reaction time, with a slight increase up to 3.4 mmol alkanes/gTOC after 4 h (Figure 6e). Hydrogen production was only observed to be significant after 4 h, reaching 15 mmol/gTOC. This hydrogen production is higher than that reported by King et al. [59] at 225 °C using Pt/C catalysts (0.4 mol hydrogen/mol levoglucosan vs 1.2 mol hydrogen/mol levoglucosan in the present work), which could be attributed to the type of support used in the current work. Thus, Oliveira et al. [60] observed an important influence of the type of carbon support, and particularly in of pH slurry of the support, in catalysts activity.

The behaviour of levoglucosan could be related to competing hydrolysis reactions taking place during heating of the feed. Thus, it has been shown that under these conditions levoglucosan can be hydrolysed to glucose [11,62]. Helle et al. [61] showed that hydrolysis begins at temperatures as low as 90 °C and can reach high reaction rate. The reaction route can be explained from the chemical pathway proposed for the transformation of glucose to sorbitol by Bindwal et al., showed in Figure 8 [62]. The hydrolysis to glucose would justify the similarity observed between levoglucosan and glucose APR results. TOC conversion was about 90 %, which can be compared with the value of 83 % observed by Irmak et al. in the APR of a 4,400 ppm glucose solution at 523K with a 5 % Pt catalyst [63]. Additionally, gas production and composition were similar to those reported by Saenz de Miera et al. [64] for the APR of 1 % glucose at similar operating conditions. Finally, Kaya et al. [65] reported 20 % H_2 in the produced gas with glucose as substrate using a 10 % Pt/AC catalyst with 13.7 nm metal nanoparticle size. The higher percentage of H_2 obtained in the current work may be due to the smaller metal nanoparticle size (d_m=2.2 nm) in the catalyst.

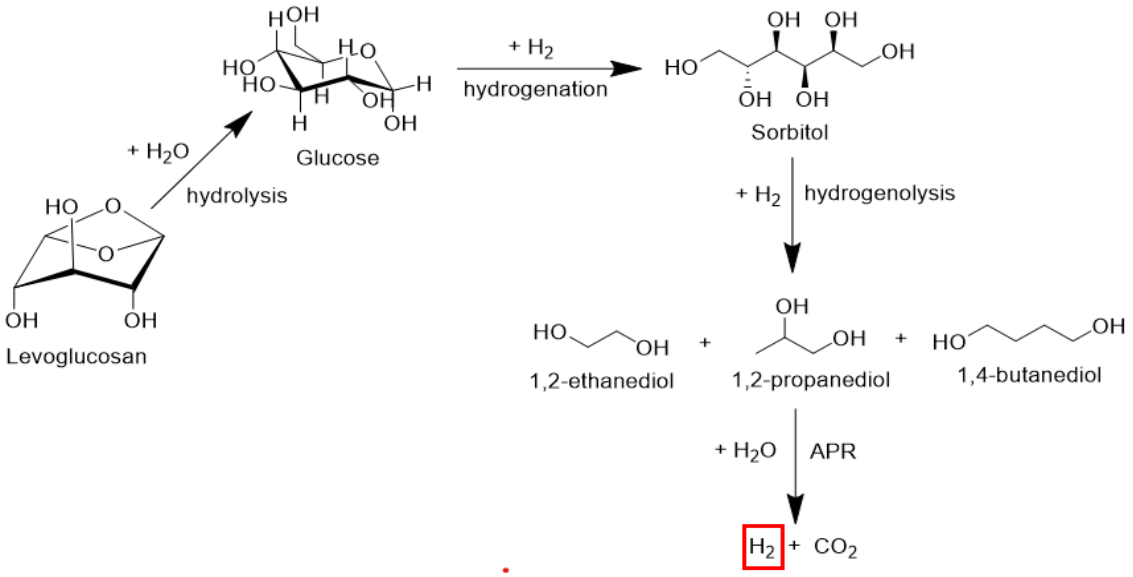

***Figure 8**: Transformation of levoglucosan into sorbitol and subsequent hydrogenolysis [57]*

In the case of acetic acid, there is a slight dependence between TOC conversion and reaction time (Figure 6c). Hydrogen production was low at all reaction times studied. On the opposite, methane production increased monotonically with time, reaching 30 mmol/gTOC after 4 h (Figure 6f). Likewise, the selectivity to methane was practically constant over time showing a mean value around 56 %. In Figure 6f it can be observed that the main gaseous product is methane, well above the hydrogen content. Pipitone et al. found an equivalent trend when using platinum-based catalyst in the APR of acetic acid [53,54]. As can be seen in the Figure 9, acetic acid is transformed into methane by APR through a simple mechanism: first, with a CO_2 removal step, and then through surface recombination [53].

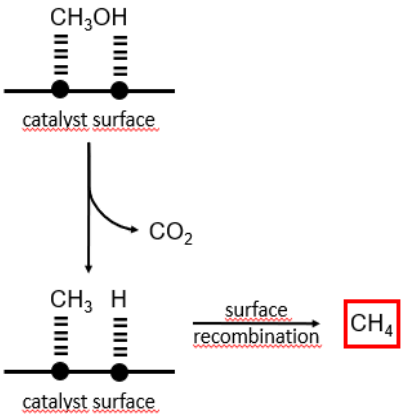

Figure 9: *Proposed reaction mechanism for the APR of acetic acid [49]*

3.3. Catalyst stability and reuse

Figure 10 shows the results for the reuse of Pt/CB catalyst in five successive 4 h runs at 220 °C, using levoglucosan as model compound. The catalyst was revealed as very stable, since only a moderate decrease of TOC conversion was observed, remaining at 74 % of initial value, after the five cycles (Figure 10a). CCgas remained almost constant at around 40-45 %, increasing very slightly with the cycles. In Figure 10b, it can be observed that the production of hydrogen increased after the first cycle (from 16 to 38 mmol/gTOC), stabilizing at a value of 35 mmol/gTOC after the fifth cycle. In the case of alkanes, generation remained constant in ca. 4 mmol/gTOC. Pipitone et al. [66] also found an improvement in hydrogen selectivity after the second reuse cycle, in the APR of alginate 1 % (wt.), using a commercial 3% Pt/C.

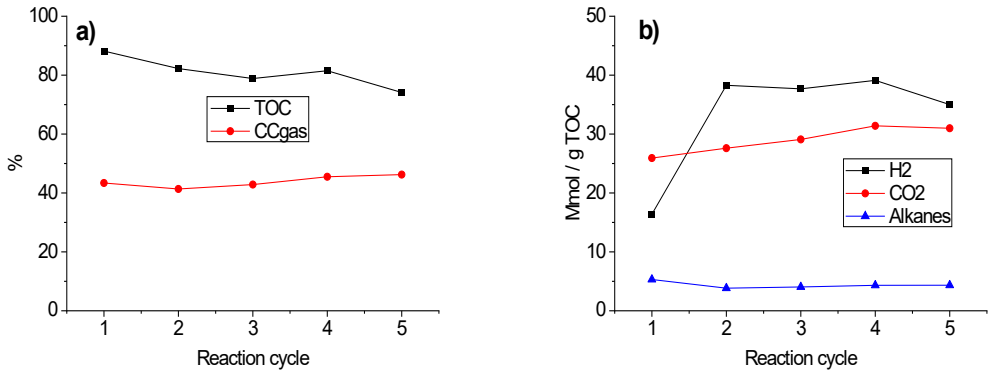

Figure 10: *Pt/CB catalyst stability in five consecutive batch reaction cycles: a) TOC conversion and CCgas, b) Gas production (1 % levoglucosan, 220 °C, 4 h)*

For a better understanding of the catalyst performance during the five cycles of reuse, it was characterized by STEM, TGA and XPS. Figure 11 shows the results of STEM characterization of the Pt/CB catalyst both fresh and used after 1, 3 and 5 cycles.

405
406
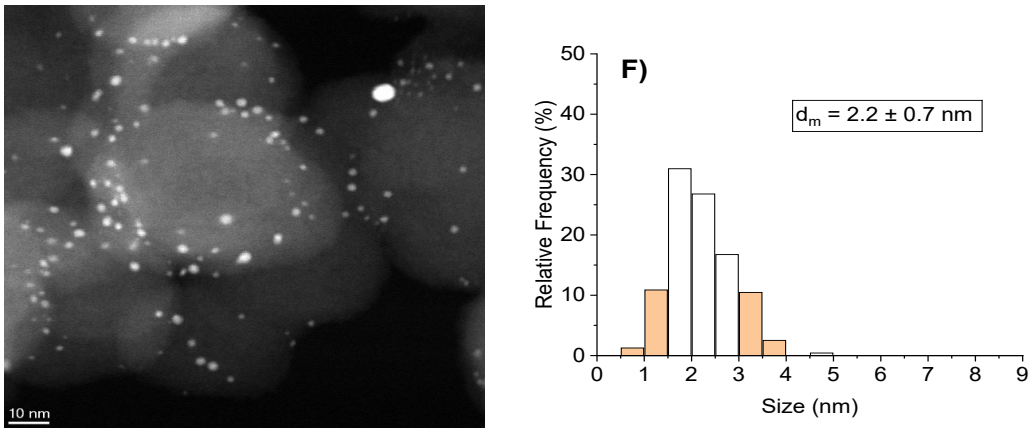

407
408
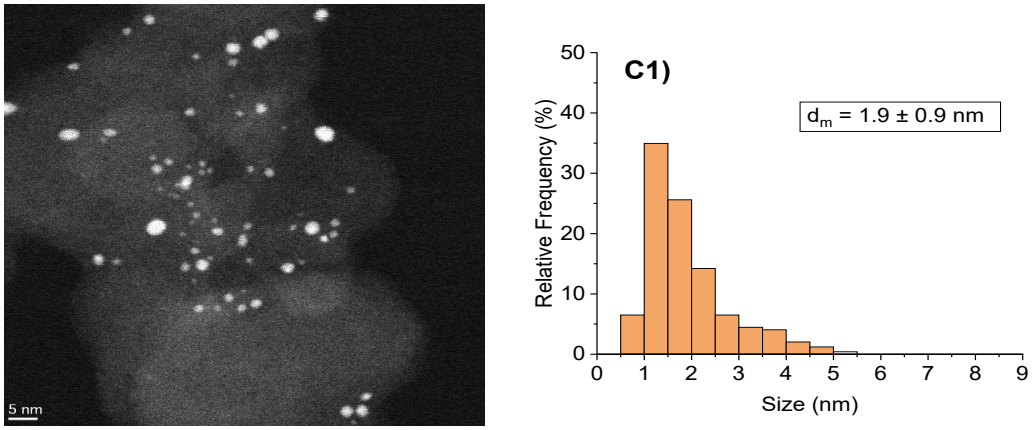

409
410
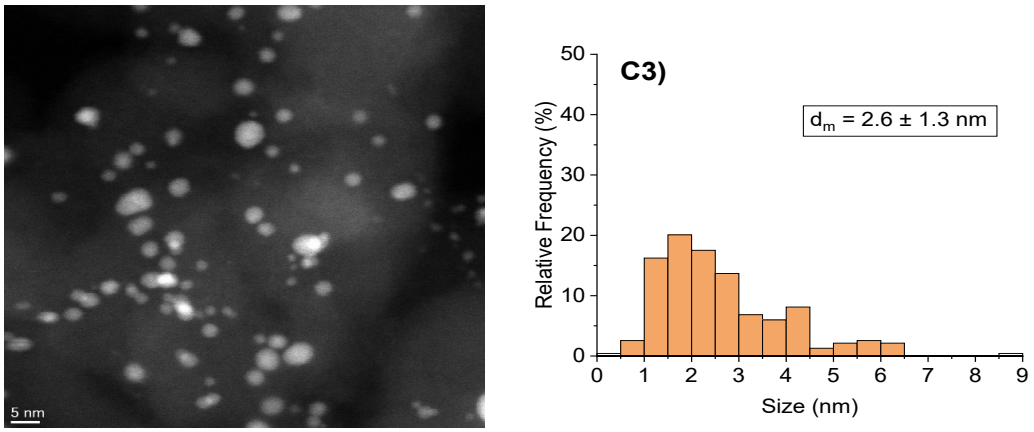

411
412
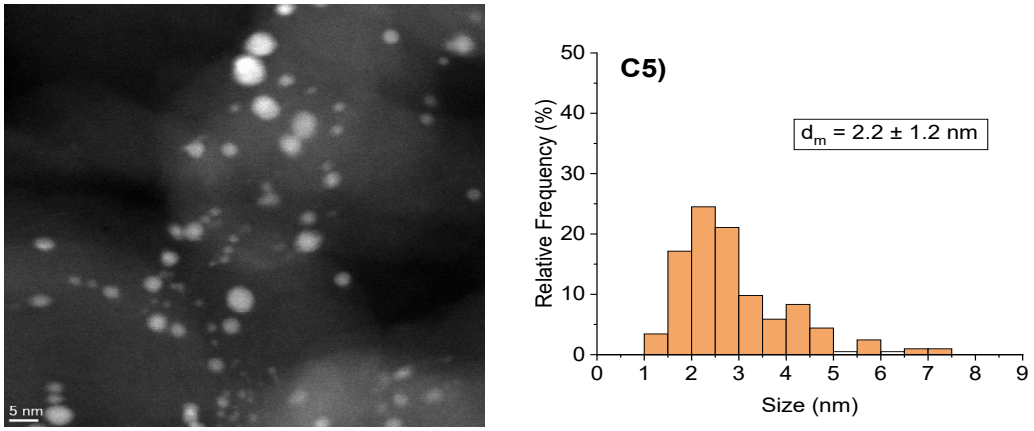

Figure 11: *STEM images of Pt/CB catalyst: F) fresh, C1) cycle 1, C3) cycle 3 and C5) cycle 5*

Well dispersed metal particles can be observed in the images and minor differences were found between fresh and reused catalyst, which allows to rule out relevant sintering influencing Pt catalytic behaviour. However, for the fresh catalyst a narrower nanoparticle size distribution ranging from 0.5 to 4 nm was observed. Some redispersion of the metal phase can be observed after 1 cycle, leading to a higher prevalence of nanoparticles smaller than 2 nm. Within the 5-cycle range studied the catalyst mean nanoparticle size remained around 2 nm but distribution became broader, with a tail extending up to 7.5 nm for the catalysts used in three and five cycles. The increase in the fraction of nanoparticles with larger size can be related to Ostwald ripening, in which growth of nanoparticles takes place because large particles are more energetically favoured than small ones [67].

As can be seen in Figure 12, thermogravimetric desorption and oxidation profiles in air were obtained with no remarkable results except a very slight weight loss in inert atmosphere at 500-600 °C, probably due to the deposition of hydrothermal carbon or coke formed during APR on the catalyst surface. The deposition of coke can contribute to lower activity since TOC conversion was found to decrease [41]. TPO profile for the fresh catalyst show a high stability in air, ascribable to the highly ordered structure of the ENSACO 250G support, with negligible mass loss ascribed to oxidation up to ca. 400°C. Likewise, TEM images do not indicate degradation of carbon support leading to evident morphological changes and changes in metallic phase dispersion.

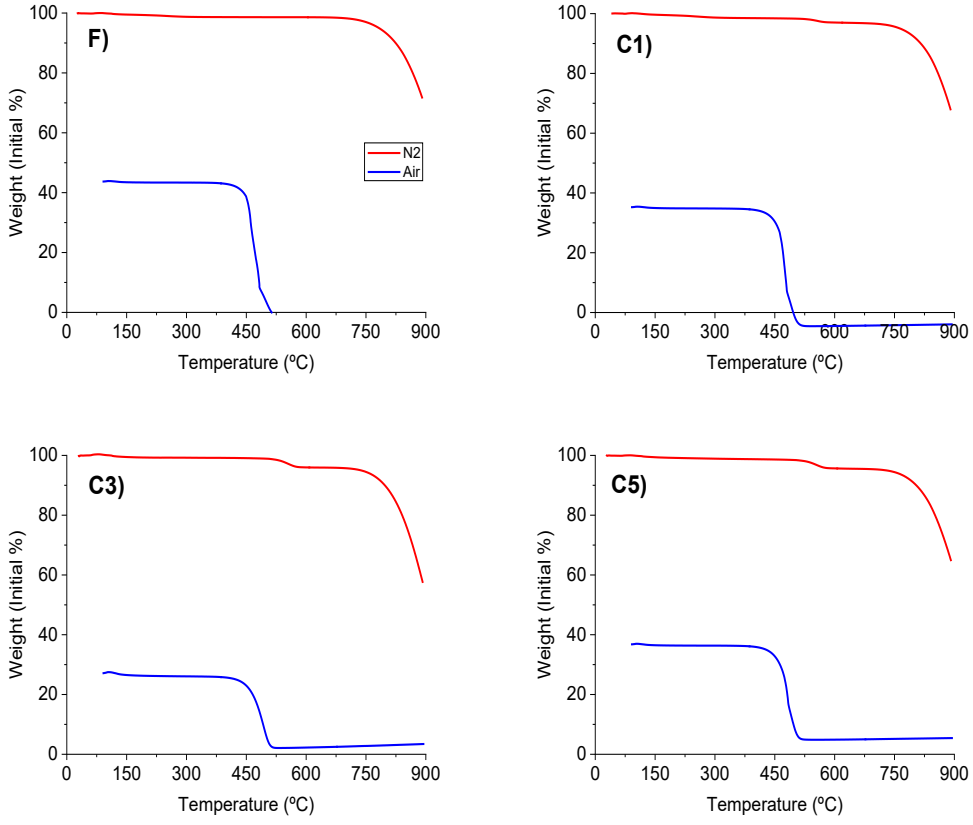

Figure 12: *Thermogravimetric analysis (desorption and oxidation) of Pt/CB catalyst: F) fresh, C1) cycle 1, C3) cycle 3 and C5) cycle 5*

Deconvoluted Pt 4f XPS spectra of fresh catalyst and catalysts used in several reaction cycles are shown in Figure 13, where peaks located at binding energy values around 71 and 75 eV are ascribed to metallic platinum, while those around 73 and 76 eV correspond to Pt^{2+} for the two spin-orbit splits (Pt $4f_{7/2}$ and Pt $4f_{5/2}$) [68]. Binding energy values and Pt^{2+}/Pt^{0} ratios calculated from the intensity of the peaks for fresh and used catalyst are summarized in Table 5. It has been reported in literature [69-71] that changes in Pt nanoparticle size can induce changes in binding energy and Pt^{2+}/Pt^{0} ratio and, in turn, higher charged metal nanoparticles induce higher catalytic activity. However, in this work no significant trend and changes in binding energies can be observed, indicating that charge transfer properties are not modified significantly along the cycles and may not be related to changes in hydrogen production. Likewise, changes observed in Pt^{2+}/Pt^{0} ratio may be related to the redispersion of the metal phase that can be observed in Figure 11, particularly after cycle 1 and most probably due to Ostwald ripening, result in a higher prevalence of low coordination sites such as corners and edges.

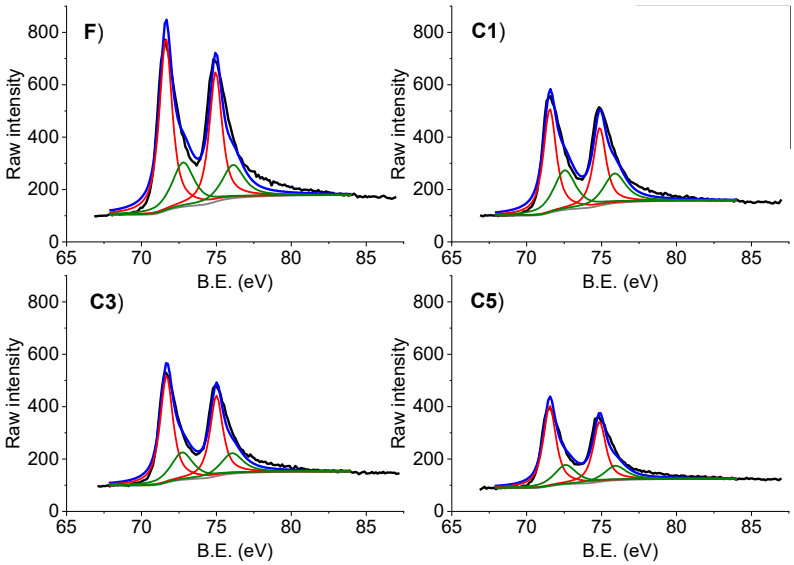

Figure 13: *Platinum (Pt 4f) XPS spectra of Pt/CB catalyst: F) fresh, C1) cycle 1, C3) cycle 3 and C5) cycle 5*

Table 5: *Binding energies (BE) for each species of Pt/C and Pt^{2+}/Pt^{0} ratios from Pt 4f XPS spectra for fresh and reused catalyst.*

Sample	Species	Binding energy (eV)		Pt^{2+}/Pt^{0} ratio
		Pt $4f_{7/2}$	Pt $4f_{5/2}$	
Fresh catalyst	Pt^{0}	71.62	74.95	0.4
	Pt^{2+}	72.78	76.11	
After cycle 1	Pt^{0}	71.54	74.89	0.7
	Pt^{2+}	72.54	75.87	
After cycle 3	Pt^{0}	71.67	75.00	0.4
	Pt^{2+}	72.71	76.04	
After cycle 5	Pt^{0}	71.53	75.86	0.4
	Pt^{2+}	72.59	75.92	

To deepen on the influence of Pt dispersion on the catalytic performance, a five-cycle reuse test was carried out using a fresh catalyst that was reduced for an additional hour previous to use. In this case, the fresh catalyst showed a nanoparticle size distribution displaced to smaller values (Figure 15) and slightly higher Pt^{2+}/Pt^{0} ratio (Table 6). Minor changes in nanoparticle size distribution were observed after cycle 1, but again, an increase in Pt^{2+}/Pt^{0} was observed after cycle one. This catalyst showed slightly higher production of hydrogen during the first two cycles, however no significant quantitative differences were observed between the two catalysts after three cycles (Figure 14). Therefore, catalysts with higher prevalence of small nanoparticles produce more hydrogen, but this nanoparticle size range is unstable under APR reaction conditions. However, the catalysts tested show minor differences in nanoparticle size distribution and the relationship between catalytic performance and metal nanoparticle reduction degree and structure cannot be unequivocally assessed.

Table 6: *Pt^{2+}/Pt^{0} ratios from XPS characterization for fresh and used catalysts. Fresh catalyst additionally reduced.*

Sample	Pt^{2+}/Pt^{0} ratio
Fresh catalyst additionally reduced	0.6
After cycle 1	0.7
After cycle 3	0.6
After cycle 5	0.6

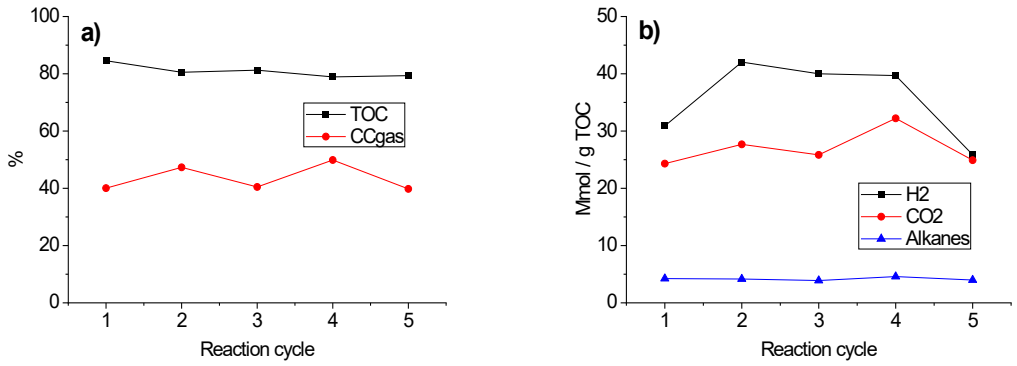

Figure 14: *Stability of additionally reduced Pt/CB catalyst in five consecutive reaction cycles a) TOC conversion and CC gas, b) Gas production (1 % levoglucosan, 220 ^{O}C, 4 h)*

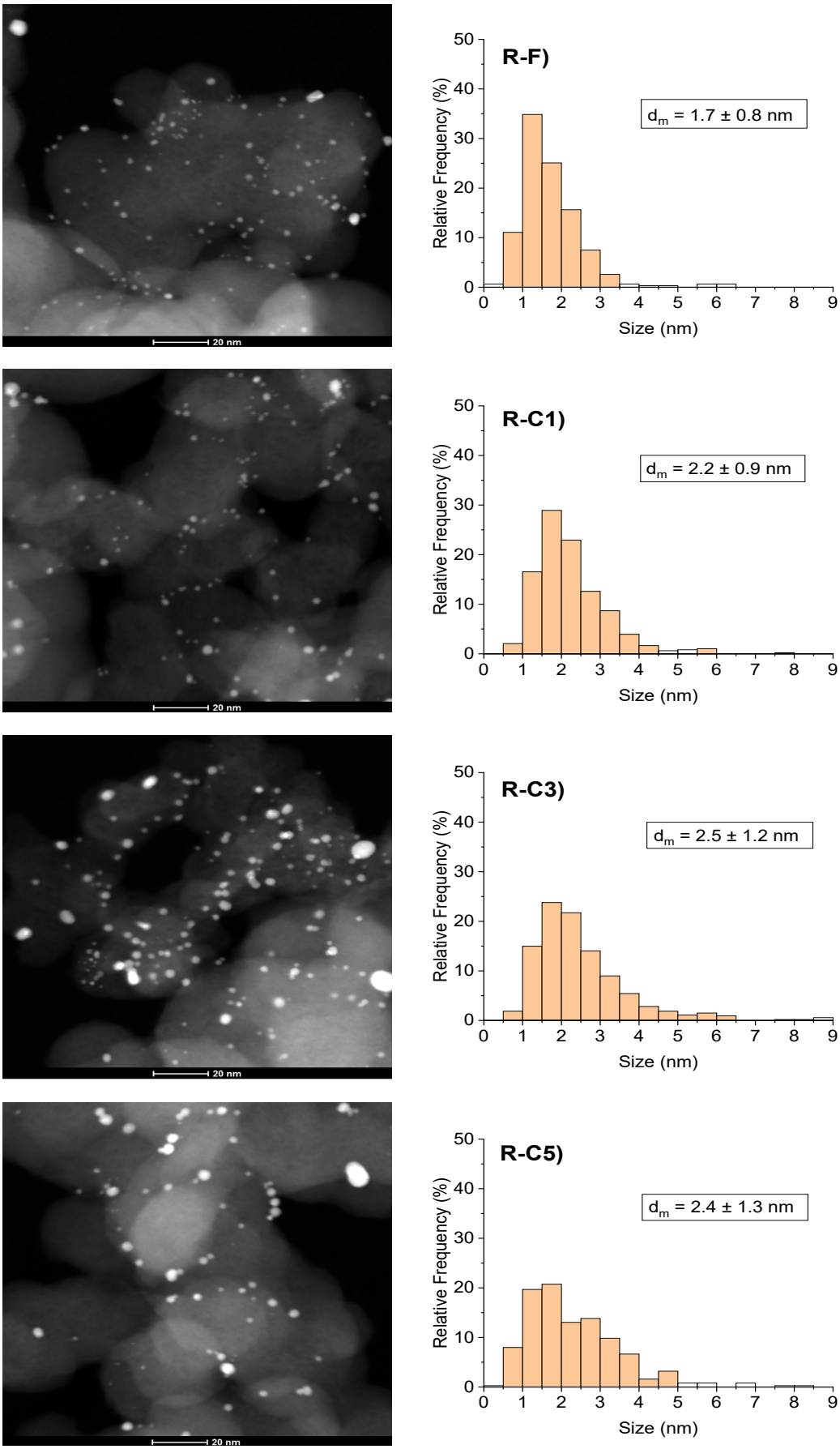

Figure 15: *STEM images of additionally reduced catalyst: F) fresh, C1) cycle 1, C3) cycle 3 and C5) cycle 5*

4. Conclusions

The APR of compounds representative of biooil aqueous fraction has been investigated with the aim to produce bio-hydrogen and/or bio-alkanes as valorization route for this wastewater biorefinery stream. The processability of model has been evaluated through substrate conversion, carbon-to-gas yield and production of hydrogen and alkanes, showing similar and even better values than those reported for common substrates used in APR such us sugars, polyols, etc. Maximum values of organic matter conversion were obtained for levoglucosan and furfural (90-95 %), being hydroxyacetone and acetic acid the more refractory (c.a 70%) in this sense. Good matching was found between conversion and carbon-to-gas yield, indicating that most of the organic matter converted follow a route to hydrogen and/or alkanes, instead of undesirable water-soluble byproducts. Accordingly, high hydrogen yields values, as high as 50 mmol/gTOC was obtained for hydroxyacetone, while acetic acid was mainly converted to methane (30 mmol/gTOC). The catalyst used showed a high stability, with nearly constant catalytic activity after 20 h of operation in five consecutive batches, which is essential for process feasibility. The results suggest that AFB fraction constitutes a promising option for bio-hydrogen production by APR.

Acknowledgements

The authors thank financial support from Community of Madrid thought research network BIO3.

References

[1] Imam, T., Capareda, S., 2012. Characterization of bio-oil, syn-gas and bio-char from switchgrass pyrolysis at various temperatures. J Anal Appl Pyrolysis 93, 170-177.

[2] Mukarakate, C., Evans, R.J., Deutch, S., Evans, T., Starace, A.K., Dam, J., Watson, M.J., Magrini, K., 2017. Reforming biomass derived pyrolysis bio-oil aqueous phase to fuels. Energy Fuels 31, 1600-1607.

[3] Rauch, R., Hrbek, J., Hofbauer, 2014. Biomass gasification for synthesis gas production and applications of the syngas. WIREs Energy Environ 3, 343-362.

[4] Larina, O.M., Sinelshchikov, V.A., Sytchev, G.A., 2016. Comparison of thermal conversion methods of different biomass types into gaseous fuel. J Phys Conf Ser 774, 012137.

[5] Fakayode, O.A., Aboagarib, E.A.A., 2020. Co-pyrolysis of lignocellulosic and macroalgae biomasses for the production of biochar – A review. Bioresour Technol 297, 122408.

[6] Pan, C., Chen, A., Liu, Z., Chen, P., Lou, H., Zheng, X., 2012. Aqueous-phase reforming of the low-boiling fraction of rice husk pyrolyzed bio-oil in the presence of platinum catalyst for hydrogen production. Bioresour Technol 125, 335-339.

[7] Li, W., Pan, C., Sheng, L., Liu, Z., Chen, P., Lou, H., Zheng, X., 2011. Upgrading of high-boiling fraction of bio-oil in supercritical methanol. Bioresour Technol 102, 9223-9228.

[8] Shemfe, M.B., Gu, S., Ranganathan, P., 2015. Techno-economic performance analysis of biofuel production and miniature electric power generation from biomass fast pyrolysis and bio-oil upgrading. Fuel 143, 361-372.

[9] Remon, J., Broust, F., Valette, J., Chhiti, Y., Alava, I., Fernandez-Akarregi, A.R., Arauzo, J., Garcia, L., 2014. Production of a hydrogen-rich gas from fast pyrolysis bio-oils: Comparison between homogeneous and catalytic steam reforming routes. Int J Hydrogen Energy 39, 171-182.

[10] Black, B.A., Michener, W.E., Ramirez, K.J., Biddy, M.J., Knott, B.C., Jarvis, M.W., Olstad, J., Mante, O.D., Dayton, D.C., Beckham, G.T., 2016. Aqueous stream characterization from biomass fast pyrolysis and catalytic fast pyrolysis. ACS Sustainable Chem Eng 4, 6815-6827.

[11] Vispute, T.P., Huber, G.W., 2009. Production of hydrogen, alkanes and polyols by aqueous phase processing of wood-derived pyrolysis oils. Green Chem 11, 1433–1445.

[12] Valle, B., Remiro, A., Aguayo, A.T., Bilbao, J., Gayubo, A., 2013. Catalysts of Ni/α-Al_2O_3 and Ni/La_2 O_3- α-Al_2O_3 for hydrogen production by steam reforming of bio-oil aqueous fraction with pyrolytic lignin retention. Int J Hydrogen Energy 38, 1307-1318.

[13] Kalekar, V.N., Vaidya, P.D., 2021. Hydrogen production by reforming of sodium alginate in the liquid phase over Pt/C catalyst. Ind Eng Chem Res 60, 9755−9763.

[14] Khodabandehloo, M., Larimi, A., Khorasheh, F., 2020. Comparative process modeling and techno-economic evaluation of renewable hydrogen production by glycerol reforming in aqueous and gaseous phases. Energy Convers Manage 225, 113483.

[15] Martin, M., Grossmann, I.E., 2014. Optimal simultaneous production of hydrogen and liquid fuels from glycerol: Integrating the use of biodiesel byproducts. Ind Eng Chem Res 53, 7730-7745.

[16] Coronado, I., Stekrova, M., Reinikainen, M., Simell, P., Lefferts, L., Lehtonen, J., 2016. A review of catalytic aqueous-phase reforming of oxygenated hydrocarbons derived from biorefinery water fractions. Int J Hydrogen Energy 41, 11003-11032.

[17] Cortright, R.D., Davda, R.R., Dumesic, J.A., 2002. Hydrogen from catalytic reforming of biomass-derived hydrocarbons in liquid water. Nature 418, 964-967.

[18] Davda, R.R., Shabaker, J.W., Huber, G.W., Cortright, R.D., Dumesic, J.A., 2005. A review of catalytic issues and process conditions for renewable hydrogen and alkanes by aqueous-phase reforming of oxygenated hydrocarbons over supported metal catalysts. Appl Catal, B 56, 171-186.

[19] Xie, T., Hare, B.J., Meza-Morales, P.J., Sievers, C., Getman, R.B., 2020. Identification of the active sites in the dehydrogenation of methanol on Pt/Al2O3 catalysts. J Phys Chem C 124, 19015−19023.

[20] Harju, H., Pipitone, G., Lefferts, L., 2020. Influence of the catalyst particle size on the aqueous phase reforming of n-butanol over Rh/ZrO2. Front Chem 8, 17.

[21] Davda, R.R., Shabaker, J.W., Huber, G.W., Cortright, R.D., Dumesic, J.A., 2003. Aqueous-phase reforming of ethylene glycol on silica-supported metal catalysts. Appl Catal, B 43, 13-26.

[22] Fasolini, A., Lombardi, E., Tabanelli, T., Basile, F., 2021. Microemulsion derived titania nanospheres: An improved Pt supported catalyst for glycerol aqueous phase reforming. Nanomaterials 11, 1175.

[23] Alvear, M., Aho, A., Simakova, I.L., Grénman, H., Salmi, T., Murzin, D.Y., 2020. Aqueous phase reforming of alcohols over a bimetallic Pt-Pd catalyst in the presence of formic acid. Chem Eng J 398, 125541.

[24] Gogoi, P., Kanna, N., Begum, P., Deka, R.C., Satyanarayana, C.V.V., Raja, T., 2020. Controlling and stabilization of Ru nanoparticles by tuning the nitrogen content of the support for enhanced H2 production through aqueous-phase reforming of glycerol. ACS Catal 10, 2489-2507.

[25] Xing, R., Dgle, V.L., Flake, M., Kovarik, L., Albrecht, K.O., Deshmane, C., Dagle, R.A. Steam reforming of fast pyrolysis-derived aqueous phase oxygenates over Co, Ni, and Rh metals supported on MgAl2O4. Catal Today 269, 166−74.

[26] El Doukkali, M., Iriondo, A., Cambra, J.F., Jalowiecki-Duhamel, L., Mamede, A.S., Dumeignil, F., Arias, P.L., 2020. Pt monometallic and bimetallic catalysts prepared by acid sol–gel method for liquid phase reforming of bioglycerol. J Mol Catal A: Chem 368-369, 125-136.

[27] Irmak, S., Öztürk, I., 2010. Hydrogen rich gas production by thermocatalytic decomposition of kenaf biomass. Int J Hydrogen Energy 35, 5312-5317.

[28] Seretis, A., Tsiakaras, P., 2016. Aqueous phase reforming (APR) of glycerol over platinum supported on Al2O3 catalyst. Renewable Energy 85, 1116-1126.

[29] Pipitone, G., Zoppi, G., Pirone, R., Bensaid, S., 2022. A critical review on catalyst design for aqueous phase reforming. Int J Hydrogen Energy 47, 151-180.

[30] Kim, T., Kim, H., Jeong, K., Chae, H., Jeong, S., Lee, C., Kim, C., 2011. Catalytic production of hydrogen through aqueous-phase reforming over platinum/ordered mesoporous carbon catalysts. Green Chem 13, 1718-1728.

[31] Rahman, M.M., 2020. Aqueous-phase reforming of glycerol over carbon-nanotube-supported catalysts. Catal Lett 150, 2674–2687.

[32] Vikla, A.K.K., Simakova, I., Demidova, Y., Keim, E.G., Calvo, L., Gilarranz, M.A., Songbo He, Seshan, K., 2021. Tuning Pt characteristics on Pt/C catalyst for aqueous-phase reforming of biomass-derived oxygenates to bio-H2. Appl Catal, A 610, 117963.

[33] Kirilin, A.V., Tokarev, A.V., Kustov, L.M., Salmi, T., Mikkola, J.-P., Murzin, D.Y., 2012. Aqueous phase reforming of xylitol and sorbitol: Comparison and influence of substrate structure. Appl Catal, A 435-436, 172-180.

[34] Shabaker, J.W., Huber, G.W., Dumesic, J.A., 2004. Aqueous-phase reforming of oxygenated hydrocarbons over Sn-modified Ni catalysts. J Catal 222, 180-191.

[35] Lozano, P., Simon, A.I., Garcia, L., Ruiz, J., Oliva, M., Arauzo, J., 2021. Influence of the Ni-Co/Al-Mg catalyst loading in the continuous aqueous phase reforming of the bio-oil aqueous fraction. Processes 9, 81.

[36] Koichumanova, K., Vikla, A.K.K., Cortese, R., Ferrante, F., Seshan, K., Duca, D., Lefferts, L., 2018. In situ ATR-IR studies in aqueous phase reforming of hydroxyacetone on Pt/ ZrO2 and Pt/AlO(OH) catalysts: The role of aldol condensation. Appl Catal, B 232, 454-463.

[37] Arandia, A., Coronado, I., Remiro, A., Gayubo, A.G., Reinikainen, M., 2019. Aqueous-phase reforming of bio-oil aqueous fraction over nickel-based catalysts. Int J Hydrogen Energy 44, 13157-13168.

608 [38] Nozawa, T., Mizukoshi, Y., Yoshida, A., Naito, S., 2014. Aqueous phase reforming of ethanol
609 and acetic acid over TiO2 supported Ru catalysts. Appl Catal, B 146, 221-226.

610 [39] Wei, Y., Lei, H., Liu, Y., Wang, L., Zhu, L., Zhang, X., Yadavalli, G., Ahring, B., Chen, S., 2014.
611 Renewable hydrogen produced from different renewable feedstock by aqueous-phase
612 reforming process. J Sustain Bioenergy Syst 4, 113-127.

613 [40] Lemus, J., Bedia, J., Calvo, L., Simakova, I.L., Murzin, D.Y., Etzold, B.J.M., Rodriguez, J.J.,
614 Gilarranz, M.A., 2016. Improved synthesis and hydrothermal stability of Pt/C catalysts based on
615 size-controlled nanoparticles. Catal Sci Technol 6, 5196-5206.

616 [41] Oliveira, A.S., Cordero-Lanzac, T., Baeza, J.A., Calvo, L., Heras, F., Rodriguez, J.J., Gilarranz,
617 M.A., 2021. Continuous aqueous phase reforming of a synthetic brewery wastewater with Pt/C
618 and PtRe/C catalysts for biohydrogen production. Chemosphere 281, 130885.,

619 [42] Alonso, N., Gilarranz, M.A., Heras, F., Rodriguez, J.J., Eser, S., 2011. Effects of Heat
620 Treatment on the Structure of LDPE-Derived Solid Carbons. Chem Eng J 172 (2-3), 1126-1136.

621 [43] Ángeles-Pascual, A., 2021. Structural atomic study in platinum heterogeneous catalyst by
622 aberration-corrected STEM. Appl Surf Sci 566, 150745

623 [44] Zhan, T., Wu, S., Ma, H., Yue, C., Huang, Z., Liu, W., Teng, J., Li, D., Wang, S., Tan, H., 2019.
624 Production of biofuel intermediates from furfural via aldol condensation over K2O clusters
625 containing N-doped porous carbon materials with shape selectivity. Microporous Mesoporous
626 Mater 281, 101-109.

627

628 [45] Simsir, H., Eltugral, N., Karagoz, S., 2017. Hydrothermal carbonization for the preparation
629 of hydrochars from glucose, cellulose, chitin, chitosan and wood chips via low-temperature and
630 their characterization. Bioresour Technol 246, 82-87.

631 [46] Chen, A., Chen, P., Cao, D., Lou, H., 2015. Aqueous-phase reforming of the low-boiling
632 fraction of bio-oil for hydrogen production: The size effect of Pt/Al2O3. Int J Hydrogen Energy
633 40, 14798-14805.

634 [47] Shao, Y., Hu, X., Zhang, Z., Sun, K., Gao, G., Wei, T., Zhang, S., Hu, S., Xiang, J., Wang, Y.,
635 2019. Direct conversion of furfural to levulinic acid/ester in dimethoxymethane: Understanding
636 the mechanism for polymerization. Green Energy Environ 4, 400-413.

637 [48] Luo, N., Fu, X., Cao, F., Xiao, T., Edwars, P.P., 2008. Glycerol aqueous phase reforming for
638 hydrogen generation over Pt catalyst – Effect of catalyst composition and reaction conditions.
639 Fuel 87, 3483-3489.

640 [49] Wang, Y., Zhao, D., Rodriguez-Padron, D., Len, C., 2019. Recent advances in catalytic
641 hydrogenation of furfural. Catalysts 9, 796.

642 [50] Sladkovskiy, D.A., Godina, L.I., Semikin, K.V., Sladkovskaya, E.V., Smirnova, D.A., Murzin,
643 D.Y., 2018. Process design and techno-economical analysis of hydrogen production by aqueous
644 phase reforming of sorbitol. Chem Eng Res Des 134, 104-116.

645 [51] Subramanian, N.D., Callison, J., Catlow, C.R.A., Wells, P.P., Dimitratos, N., 2016. Optimised
646 hydrogen production by aqueous phase reforming of glycerol on Pt/Al2O3. Int J Hydrogen
647 Energy 41, 18441-18450.

[52] Aho, A., Rosales, C., Eränen, K., Salmi, T., Murzin, D.Y., Grenman, H., 2020. Biohydrogen from dilute side streams - Influence of reaction conditions on the conversion and selectivity in aqueous phase reforming of xylitol. Biomass Bioenergy 138, 105590.

[53] Pipitone, G., Zoppi, G., Bocchini, S., Rizzo, A.M., Chiaramontic, D., Pirone, R., Bensaid, S., 2020. Aqueous phase reforming of the residual waters derived from lignin-rich hydrothermal liquefaction: investigation of representative organic compounds and actual biorefinery streams. Catal Today 345, 237-250.

[54] Pipitone, G., Zoppi, G., Ansaloni, S., Bocchini, S., Deorsola, F.A., Pirone, R., Bensaid, S., 2019. Towards the sustainable hydrogen production by catalytic conversion of C-laden biorefinery aqueous streams. Chem Eng J 377, 120677.

[55] Callison, J., Subramanian, N.D., Rogers, S.M., Chutia, A., Gianolio, D., Catlow, C.R.A., Wells, P.P., Dimitratos, N., 2018. Directed aqueous-phase reforming of glycerol through tailored platinum nanoparticles. Appl Catal B 238, 618-628.

[56] Rahman, M.M., 2015. H2 production from aqueous-phase reforming of glycerol over Cu-Ni bimetallic catalysts supported on carbon nanotubes. Int J Hydrogen Energy 40, 14833-14844.

[57] Dietrich, P.J., Lobo-Lapidus, R.J., Wu, T., Sumer, A., Akatay, M.C., Fingland, B.R., Guo, N., Dumesic, J.A., Marshall, C.L., Stach, E., Jellinek, J., Delgass, W.N., Ribeiro, F.H., Miller, J.T., 2012. Aqueous phase glycerol reforming by PtMo bimetallic nano-particle catalyst: Product selectivity and structural characterization. Top Catal 55, 53-69.

[58] Zhang, L., Karim, A.M., Engelhard, M.H., Wei, Z., King, D.L., Wang, Y., 2012. Correlation of Pt–Re surface properties with reaction pathways for the aqueous-phase reforming of glycerol. J Catal 287, 37-43.

[59] King, D., Wang, Y., Zhang, L., Karim, A., Heldebrant, D., 2011. Biomass-derived liquids distributed (aqueous phase) reforming. DOE Hydrogen and fuel cells program review (May 10, 2011).

[60] Oliveira, A.S., Baeza, J.A., Calvo, L., Alonso-Morales, N., Heras, F., Rodriguez, J.J., Gilarranz, M.A., 2019. Production of hydrogen from brewery wastewater by aqueous phase reforming with Pt/C catalysts. Appl Catal B 245, 367-375.

[61] Helle, S., Bennett, N.M., Lau, K., Matsui, J.H., Duff, S.J.B., 2007. A kinetic model for production of glucose by hydrolysis of levoglucosan and cellobiosan from pyrolysis oil. Carbohydr Res 342, 2365-2370.

[62] Bindwal, A.B., Vaidya, P.D., 2013. Kinetics of aqueous-phase hydrogenation of levoglucosan over Ru/C catalyst. Ind Eng Chem Res 52, 17781−17789.

[63] Irmak, S., Meryemoglu, B., Ozsel, B.K., Hasanoglu, A., Erbatur, O., 2015. Improving activity of Pt supported metal catalysts by changing reduction method of Pt precursor for hydrogen production from biomass. Int J Hydrogen Energy 40, 14826-14832.

[64] Saenz de Miera, B., Oliveira, A.S., Baeza, J.A., Calvo, L., Rodriguez, J.J., Gilarranz, M.A., 2020. Treatment and valorisation of fruit juice wastewater by aqueous phase reforming: Effect of pH, organic load and salinity. J Cleaner Prod 252, 119849.

687 [65] Kaya, B., Irmak, S., Hasanoglu, A., Erbatur, O., 2015. Developing Pt based bimetallic and
688 trimetallic carbon supported catalysts for aqueous-phase reforming of biomass-derived
689 compounds. Int J Hydrogen Energy 40, 3849-3858.

690 [66] Pipitone, G., Tosches, D., Bensaid, S., Galia, A., Pirone, R., 2018. Valorization of alginate for
691 the production of hydrogen via catalytic aqueous phase reforming. Catal Today 304, 153-164

692 [67] Neumann, S., Schröder, J., Bizzoto, F., Arenz, M., Dworzak, A., Oezaslan, M., Bäumer, M.,
693 Kunz, S., 2019. Halide-induced leaching of Pt nanoparticles – Manipulation of particle size by
694 controlled Ostwald ripening. Chem Nano Mat 5, 462-471.

695 [68] Álvarez-Montero, M.A., Gómez-Sainero, L.M., Mayoral, A., Diaz, I., Baker, R.T., Rodriguez,
696 J.J., 2011. Hydrodechlorination of chloromethanes with a highly stable Pt on activated carbon
697 catalyst. J Catal 279, 389-396.

698 [69] Gurevich, S.A., Il'yushchenkov, D.S., Yavsin, D.A., Glebova, N.V., Nechitailov, A.A., Zelenina,
699 N.K., Tomasov, A.A., 2017. Charge state and activity of Pt/C catalysts in oxygen reduction
700 reaction. Russian J Electrochem 53, 6, 567–574.

701 [70] Yan, QQ., Wu, DX., Chu, SQ., Chen, ZQ., Lin, Y., Chen, MX., Zhang, J., Wu, XJ., Liang, HW.,
702 2019. Reversing the charge transfer between platinum and sulfur-doped carbon support for
703 electrocatalytic hydrogen evolution. Nat Commun 10, 4977.

704 [71] Elangovan A., Xu, J., Sekar, A., Rajendran, S., Liu, B., Li, J., 2021. Platinum deposited nitrogen-
705 doped vertically aligned carbon nanofibers as methanol tolerant catalyst for oxygen reduction
706 reaction with improved durability. Appl. Nano 2, 303–31

707